This is the preprint of an article in Computers in Biology and Medicine Vol 28 (2008) pp 727-738.

A Boundary Element Model of the Human Eye Undergoing Laser Thermokeratoplasty

Ean-Hin Ooi*, Whye-Teong Ang and Eddie-Yin-Kwee Ng
School of Mechanical and Aerospace Engineering,
Nanyang Technological University,
50 Nanyang Avenue, Singapore 639798

Abstract

In the present paper, a three-dimensional radially symmetric boundary element model of the human eye is proposed for simulating changes in corneal temperature during treatment of laser thermokeratoplasty. Energy absorption inside the cornea is modeled using the Beer-Lambert law. Heat transfer inside the eye is assumed to be governed by the classical heat diffusion equation. The resulting initial-boundary value problem is solved numerically using a time-stepping boundary element method. The temperature field is calculated for heating by both the pulsed laser and the continuous wave laser. The results obtained are compared with those from other models found in the literature.

Keywords: laser thermokeratoplasty, boundary element method, pulsed laser, continuous wave laser, temperature.

* Author for correspondence (E. H. Ooi)
Tel: +65 67904004
E-mail: L050016@ntu.edu.sg

1 Introduction

Laser thermo-keratoplasty (L-TKP) is a corneal refractive surgery technique intended for vision correction. In L-TKP, the human cornea is shrunk to a certain size in order to improve its refractive power. Shrinkages are induced thermally through laser heating. Although successful applications of the L-TKP have been documented in the past, it is not the preferred choice for clinical treatment of hyperopia compared to photo-refractive keratectomy and laser in-situ keratomileusis. This is largely due to the low predictability and repeatability of the L-TKP in producing reliable results. Nevertheless, L-TKP is still popular in the treatment of presbyopic patients today [1].

During the last decade or so, numerous investigations have been carried out to study the thermo-mechanical behaviors of the human cornea during treatment of L-TKP to improve its predictability and the repeatability. Since L-TKP may cause thermal damage to the cornea, most of the experiments were carried out in-vitro using either the human or the animal cornea as test samples. Alternatively, some researchers have opted for mathematical investigations due to its ease of implementation. With the availability of high computing power, more realistic and sophisticated models can be developed to improve the accuracy of the simulated solution.

For mathematical convenience, many models for investigating the corneal temperature distribution during L-TKP assumed highly simplified geometries and initial-boundary conditions. Peppers *et al* [2] and Mainster [3] modeled the cornea as a half-space region where heat flow during laser heating was assumed to be one-dimensional. The absorption of laser energy inside the cornea was modeled using the Beer-Lambert law. Mainster *et al* [4] and Zhou *et al* [5] modeled the human cornea was modeled as a finite cylinder where the temperature distribution during treatment of L-TKP was calculated using the finite difference method. A similar cylindrical model solved using

the finite element method was developed by Brinkmann *et al* [6]. Unlike the models before, Brinkmann *et al* [6] accounted for the intracorneal focusing of the laser beam which was modeled based on ray tracing measurements. This model was subsequently used by Brinkmann and co-workers to investigate the thermal responses of the human cornea during L-TKP under various conditions [7], [8], [9], [10]. In [11] and [12], the cornea was modeled as a rectangular strip of finite thickness. Analytical expressions to the corneal temperature distribution during L-TKP were obtained for various conditions where solutions were computed numerically. Recently, Podol'stev and Zheltov [13] modeled the human eye as a multi-layered cylinder to study the heat transfer process during L-TKP. The laser beam which is incident at the center of the cornea was assumed to be absorbed and scattered inside each different eye region. Results obtained were used to identify the threshold conditions for photo-destruction of the human cornea.

Although models that assumed highly simplified geometry of the cornea greatly simplifies the problem, it requires assumptions to be made when specifying the boundary conditions which may not be physiologically correct. In the present study, a three-dimensional radially symmetric model of the human eye is developed which takes into account the major ocular components such as the aqueous humor, lens, vitreous and the sclera. The eye model is used to simulate the transient temperature changes inside the cornea during treatment of L-TKP. Two of the most commonly used lasers in L-TKP, namely the pulsed laser and the continuous wave laser are considered. Changes in the corneal temperature are calculated numerically using the boundary element method. Unlike the finite element method which requires a full domain discretization, only the boundary of the solution domain has to be discretized when using the boundary element method. Thus, the preparation of boundary data may be greatly simplified, especially for complicated geometries like the human eye.

The aim of the present study is to demonstrate the feasibility of using an anatomically more realistic eye model for simulating temperature changes inside the cornea during treatment of L-TKP. The thermal behaviors of the human cornea subjected to laser heating are studied. Thermally induced corneal shrinkages are qualitatively examined for both the pulsed laser and the continuous wave laser. This is carried out by comparing the spatial and temporal temperature profiles of the cornea with its shrinkage threshold temperatures reported elsewhere in the literature.

2 Laser Thermo-Keratoplasty (L-TKP)

Corneal collagen is known to shrink when heated to temperatures between 55 and 65^{o}C [14]. In practice however, the temperature which the cornea is heated to depends on the type of laser used which ultimately depends on the parameters of the laser. When the corneal temperature exceeds 90^{o}C, the collagen relaxes to counter the intended corneal shrinkage [15]. The cornea consists of three layers, namely the epithelium (the outermost layer), the stroma (the middle layer) and the endothelium (the innermost layer). During treatment of L-TKP, it is important to ensure that the temperature of the deep stromal tissues reaches the shrinkage threshold rather than the epithelial layer alone. This is to guarantee a long term effect of the corneal shrinkage [6]. The temperature at the corneal endothelium however, should not reach 65^{o}C to avoid thermal damage of the endothelial cells [16].

Lasers used in L-TKP are typically in the mid-infrared region; emitted at a wavelength of approximately 2μm. The holmium laser, Ho:YAG, is commonly used in pulsed laser treatment and has a wavelength of 2.1μm. In the continuous wave laser treatment, laser diodes which exhibit a wider range of wavelength due to its tunability are used [8]. Typical values of the laser wavelength may lie between 1.85 and 1.87μm [9].

3 The Human Eye Model

A three-dimensional radially symmetric model of the human eye which follows closely the dimensions of the model in [17] is developed. The optic nerve is excluded due to its minimal influence on the overall temperature distribution of the eye especially in the corneal region. Internal eye structures such as the aqueous humor, the lens and the vitreous are modeled based on dimensions which were obtained from anatomical measurements [18], [19]. The retina and the choroid which are relatively thin are modeled together with the sclera as one homogeneous region. The iris is also assumed to be part of the sclera since they both have similar thermal properties [20]. The human eye is modeled as comprising five distinct regions, namely the cornea, the aqueous humor, the lens, the vitreous and the sclera which we denote as R_1, R_2, R_3, R_4 and R_5 respectively.

With reference to the cylindrical polar coordinates r, θ and z, Figure 1 shows a cross-section of the model on the rz plane. (Note that r denotes the distance of a point from the z axis.) The full geometry of the model is obtained by rotating the cross-section by an angle of 360° about the z axis.

Each region of the human eye is assumed to be homogeneous and thermally isotropic. Thermal properties such as thermal conductivity, density and specific heat may be found in the literature and they are listed in Table 1.

3.1 Governing Heat Equation

The partial differential equation governing the axisymmetric heat flow inside the human eye subject to laser heating is given by

$$\rho_i c_i \frac{\partial}{\partial t}[T_i(r,z,t)] = \nabla\left(\kappa_i \nabla T_i(r,z,t)\right) + S_i(r,z,t), \quad \text{for } i = 1,2,3,4 \text{ and } 5, \tag{1}$$

where ρ_i, c_i and κ_i are respectively the density, specific heat and thermal conductivity of the region R_i, t is time, T_i is the temperature in R_i and S_i is heat absorbed by R_i during laser irradiation. Note that for the radially symmetric model, the temperature T_i is taken to be a function of r, z and t, that is, independent of the coordinate θ.

For the range of laser wavelength (1.85-2.1μm) used in the treatment of L-TKP (as mentioned in Section 2), the heat absorption S_i may be given by

$$S_i(r,z,t) = \begin{cases} \phi(t)\mu(1-\digamma)E(r)\exp(-\mu z), & \text{for } i=1, \\ 0 & \text{for } i=2,3,4 \text{ and } 5, \end{cases} \tag{2}$$

where μ is the laser absorption coefficient whose value depends on the laser wavelength, $\digamma$ is the Fresnel reflectance at the corneal surface, $E(r)$ is incident irradiance at the center of the corneal surface, and $\phi(t)$ is given by

$$\phi(t) = \begin{cases} 1 & \text{if laser is on,} \\ 0 & \text{if laser is off.} \end{cases} \tag{3}$$

According to Manns *et al* [12], the value of Fresnel reflectance, $\digamma$ is given by 0.024.

Equation (2) implies that heat from the laser energy is only absorbed inside the cornea. This assumption is based on the absorption properties of ocular media, as explained in [25]. If the laser wavelength is between 1.85 and 2.1μm, the cornea absorbs more than 95% of the laser energy. The remaining percentage of the non-absorbed energy may be assumed to be reflected from the corneal surface. Thus, no laser beam passes through the cornea into the other regions of the eye during laser irradiation.

In the present study, the laser beam profile is assumed to be of the Gaussian type. Although the actual laser beam profile may not be perfectly Gaussian, the differences are not expected to produce any significant effects on the temperature distribution inside the cornea [12]. The incident irradiance may thus be written as

$$E(r) = E_0 \exp\left(-\frac{2r^2}{w^2}\right), \tag{4}$$

where E_0 is the peak irradiance and w is the radius of laser beam at the corneal surface where the laser power decreases to $\exp(-1)$ times its maximum value.

3.2 Initial-Boundary Conditions

As shown in Figure 1, Γ_1 and Γ_2 are parts of the exterior boundary of the human eye model. Here, the conditions specified on Γ_1 and Γ_2 follow those that are reported in [17] and [26].

On the exterior surface of the cornea Γ_1, heat is transferred to the environment via convection and radiation. Cooling is aided by the evaporation of tears from the tear film on top of the corneal surface. More mathematically, this condition is given by

$$-\kappa_1 \frac{\partial T_1}{\partial n} = h_{\text{amb}} \left(T_1 - T_{\text{amb}}\right) + \varepsilon\sigma \left(T_1^4 - T_{\text{amb}}^4\right) + E_{\text{vap}} \quad \text{on } \Gamma_1, \tag{5}$$

where the first, second and last term on the right hand side refers to the heat loss due to convection, radiation and tears evaporation respectively, h_{amb} is ambient convection coefficient, T_{amb} is ambient temperature, ε is corneal emissivity, σ is the Stefan-Boltzmann constant, E_{vap} is the heat loss due to tears evaporation and $\partial T_1/\partial n$ is the rate of change of T_1 in the outward unit vector normal to the external corneal surface Γ_1.

On the exterior surface of the sclera Γ_2, heat from blood flow across the sclera enters the eye and diffuses via conduction to the corneal surface. Thus, we may write

$$-\kappa_5 \frac{\partial T_5}{\partial n} = h_{\text{bl}} \left(T_5 - T_{\text{bl}}\right) \quad \text{on } \Gamma_2, \tag{6}$$

where h_{bl} is the blood convection coefficient, T_{bl} is the blood temperature and $\partial T_5/\partial n$ denotes the rate of change of T_5 in the outward unit vector normal to the external corneal surface Γ_2.

At the interfaces between two contiguous regions of the human eye, the continuity principle applies such that

$$
\begin{aligned}
T_1 = T_2 \text{ and } \kappa_1 \frac{\partial T_1}{\partial n} &= \kappa_2 \frac{\partial T_2}{\partial n} \text{ on } I_{12}, \\
T_1 = T_5 \text{ and } \kappa_1 \frac{\partial T_1}{\partial n} &= \kappa_5 \frac{\partial T_5}{\partial n} \text{ on } I_{15}, \\
T_2 = T_3 \text{ and } \kappa_2 \frac{\partial T_2}{\partial n} &= \kappa_3 \frac{\partial T_3}{\partial n} \text{ on } I_{23}, \\
T_2 = T_5 \text{ and } \kappa_2 \frac{\partial T_2}{\partial n} &= \kappa_5 \frac{\partial T_5}{\partial n} \text{ on } I_{25}, \\
T_3 = T_4 \text{ and } \kappa_3 \frac{\partial T_3}{\partial n} &= \kappa_4 \frac{\partial T_4}{\partial n} \text{ on } I_{34}, \\
T_3 = T_5 \text{ and } \kappa_3 \frac{\partial T_3}{\partial n} &= \kappa_5 \frac{\partial T_5}{\partial n} \text{ on } I_{35}, \\
T_4 = T_5 \text{ and } \kappa_4 \frac{\partial T_4}{\partial n} &= \kappa_5 \frac{\partial T_5}{\partial n} \text{ on } I_{45},
\end{aligned} \tag{7}
$$

where I_{ij} denotes the interface between R_i and R_j and $\partial T_i/\partial n$ (at the interface) denotes the rate of change of temperature T_i in the direction of a normal vector to the interface.

The values of the various parameters in (5) and (6) are the same as those in [17] and they are listed in Table 2.

The initial condition is given by the steady-state temperature prior to laser heating, that is, by the solution obtained from solving the steady-state heat equation

$$
\nabla \left(\kappa_i \nabla T_i(r, z) \right) = 0 \quad \text{for } i = 1, 2, 3, 4 \text{ and } 5, \tag{8}
$$

subject to (5), (6) and (7).

4 Boundary Element Model

The numerical solution of (1) subjected to the conditions in (5), (6), (7) and (8) is obtained using a time-stepping dual-reciprocity boundary element

method. To do so, an integro-differential formulation of (1) with reference to the region R_i in the cross-section of the human eye model in Figure 1, that is,

$$\begin{aligned}\gamma(\xi,\eta)T_i(\xi,\eta,t) = &\int_{\Lambda_i} T_i(r,z,t)\frac{\partial}{\partial n}[\Phi(r,z;\xi,\eta)]\cdot r\cdot ds(r,z)\\ &-\int_{\Lambda_i}\Phi(r,z;\xi,\eta)\frac{\partial}{\partial n}[T_i(r,z,t)]\cdot r\cdot ds(r,z)\\ &+\iint_{R_i}\Phi(r,z;\xi,\eta)\left[\frac{\rho_i c_i}{\kappa_i}\frac{\partial}{\partial t}[T_i(r,z,t)]-\frac{1}{\kappa_i}S_i(r,z,t)\right]dR(r,z)\\ &\qquad\text{for } (\xi,\eta)\in R_i\cup\Lambda_i \text{ and } i=1,2,3,4 \text{ and } 5, \end{aligned}\tag{9}$$

where Λ_i denotes the curve boundary of the region R_i, $ds\,(r,z)$ denotes the length of an infinitesimal part of curve Λ_i and $dR(r,z)$ denotes the area of an infinitesimal portion of the region R_i, $\gamma(\xi,\eta)=1$ if (ξ,η) lies in the interior of R_i, $\gamma(\xi,\eta)=1/2$ if (ξ,η) lies on a smooth part of Λ_i, and $\Phi\,(r,z;\xi,\eta)$ and $\partial\Phi\,(r,z;\xi,\eta)\,/\partial n$ are the axisymmetric fundamental solution of the Laplace equation and its normal derivative respectively, given by

$$\begin{aligned}\Phi(r,z;\xi,\eta) &= -\frac{K(m(r,z;\xi,\eta))}{\pi\sqrt{a(r,z;\xi,\eta)+b(r;\xi)}},\\ \frac{\partial}{\partial n}[\Phi(r,z;\xi,\eta)] &= -\frac{1}{\pi\sqrt{a(r,z;\xi,\eta)+b(r;\xi)}}\\ &\quad\times\{\frac{n_r}{2r}[\frac{\xi^2-r^2+(\eta-z)^2}{a(r,z;\xi,\eta)-b(r;\xi)}E(m(r,z;\xi,\eta))\\ &\quad-K(m(r,z;\xi,\eta))]\\ &\quad+n_z\frac{\eta-z}{a(r,z;\xi,\eta)-b(r;\xi)}E(m(r,z;\xi,\eta))\},\\ m(r,z;\xi,\eta) &= \frac{2b(r;\xi)}{a(r,z;\xi,\eta)+b(r;\xi)},\\ a(r,z;\xi,\eta) &= \xi^2+r^2+(\eta-z)^2,\quad b(r;\xi)=2r\xi\end{aligned}\tag{10}$$

where n_r and n_z are the components of the outward unit normal vector on Λ_i in the r and z direction respectively and K and E denotes the complete elliptic integral of the first and second kind respectively as defined in [27]. Note that in the axisymmetric formulation, the z axis does not form part of the curve boundary Λ_i. Details on the derivation of (9) and (10) may be found in [28]. The boundary element method is implemented by discretizing the boundary Λ_i into small straight line segments. The domain integral and the time dependent variable in (9) are treated using the dual-reciprocity boundary element method (DR-BEM) and the time stepping scheme respectively. For a detailed derivation, one may refer to the Appendix.

5 Results and Analysis

In the actual clinical treatment of L-TKP, the cornea is heated at eight different spots which are arranged in an annular pattern about the center of the corneal surface. In the present study, only one spot which is located at the center of the corneal surface is considered. This assumption is necessary to maintain the radially symmetric feature of the human eye which is of great computational advantage. With this assumption, an increase in the temperature near the center of the corneal surface is to be expected.

To capture accurately the large thermal variation over the small heated area on the corneal surface, the boundary discretization there should be sufficiently fine. Similarly, a large number of interior collocation points must be chosen inside the cornea and aqueous humor since temperature varies greatly around these regions (see the Appendix). The boundaries of the human eye model are discretized into a total of 253 boundary elements, with 72 of them located on the boundary of the cornea. A total of 316 interior points is selected inside the human eye model, with 53 and 142 of them placed inside the cornea and aqueous humor respectively. The interior points are

selected such that they are densely packed in regions close to the point where the laser beam is incident. This is shown in Figure 2. The system of linear algebraic equations in the time-stepping DR-BEM is set up using Matlab 6.5© [29]. Simulations are executed on a Pentium 2.4GHz, 512MB RAM personal computer.

Before simulations can be carried out, the laser absorption coefficient, μ in the cornea has to be chosen. In the present study, as in [13], μ is taken to be that of water. In addition, its value is assumed to be independent of temperature. The radius of the laser beam, w is chosen to be 0.3mm which is typical in a clinical treatment of L-TKP [11].

5.1 Pulsed laser irradiation

The values of each laser parameter chosen for the pulsed laser treatment are summarized in Table 3. Energy per pulse denotes the amount of energy supplied by the laser beam to the cornea. Pulse duration indicates the duration when the laser beam is incident on the surface of the cornea and pulse repetition rate defines the number of pulses that is applied onto the cornea every 1 second. According to Manns *et al* [11], a typical pulsed L-TKP treatment consists of seven laser pulses which we will consider here. Each laser pulse is applied every 0.2s (pulse repetition rate) for a duration of 200μs (pulse duration).

It follows that the function $\phi(t)$ defined in (3) may be written as

$$\phi(t) = \begin{cases} 1 & \text{if } t \in J, \\ 0 & \text{if } t \notin J, \end{cases} \tag{11}$$

where t is the time taken to be in seconds here and J is the time interval defined by

$$J = \bigcup_{m=0}^{6} \{t \ : 0.2002m \leq t \leq 0.2002m + 0.0002\}. \tag{12}$$

Figure 3 plots the corneal temperature against time at various points along the pupillary axis ($r = 0$) during the course of pulsed L-TKP. Seven temperature peaks corresponding to the seven laser pulses can be observed. During the 0.2s time interval when the cornea is not irradiated, the heat absorbed inside the cornea is diffused into the environment via convection and radiation and into the remaining part of the eye via conduction. This is shown in Figure 3 by the rapid decrease in temperature following each temperature peak.

At the end of the seventh pulse, temperature at $(r, z) = (0, 0)$ is approximately 111°C. At the interface between the cornea and aqueous humor, that is, at $(r, z) = (0, 588\mu\text{m})$, the temperature approximately 53°C . According to Brinkmann *et al* [7], when using pulsed laser, the cornea should be heated to a minimum temperature of 100°C to initiate the shrinking process. Based on the temperature plot in Figure 3, this requirement is satisfied at the surface of the cornea.

Figure 4 shows the variation of the corneal temperature along the pupillary axis (against z at $r = 0$) following each laser pulse. The vertical lines drawn at $z = 50\mu$m and $z = 550\mu$m separate the plotted area into the corneal epithelium ($z < 50\mu$m), corneal stroma ($50\mu\text{m} < z < 550\mu\text{m}$) and corneal endothelium ($z > 550\mu$m). Temperature thresholds denoting the lower limit for corneal shrinkage ($T = 55$°C) and the limit for corneal relaxation ($T = 90$°C) are indicated by the horizontal lines.

Throughout the course of pulsed L-TKP treatment, the most of the corneal stroma temperature is found to lie between 55 and 90°C (see Figure 4). This is suitable for inducing corneal shrinkages. Although a small region inside the stroma ($50\mu\text{m} \leq z \leq 100\mu\text{m}$) is heated beyond its relaxation threshold, overall shrinkage of the cornea may not be severely affected since relaxation occur only at superficial depths of the stroma. Similarly, the corneal endothelium ($z > 550\mu$m) which has a temperature below the 55°C

threshold may not have severe effects on the corneal shrinkage in general. This is due to the absence of collagen fibers in the corneal endothelium [30]. The temperature reached by the corneal endothelium also implies that no endothelial cell damage occurs during the course of pulsed L-TKP [16] (see section 2).

The spatial temperature profiles over a small cross-section of the human eye on the rz plane are shown in Figure 5. The cross-section which comprises mainly the cornea and the aqueous humor is selected in such a way that a significant variation in the temperature can be observed. For a clearer visualization, the temperature plots in Figure 1 are given with the mirror images about the z axis. The dotted line indicates the interface between the cornea and the aqueous humor.

5.2 Continuous wave laser irradiation

Table 4 summarizes the values of laser parameters chosen for the continuous wave L-TKP. Similar to the pulsed laser treatment, the values given in Table 4 represent values in a typical clinical treatment. Unlike pulsed laser treatment, the continuous wave laser irradiates the surface of the cornea in a continuous manner over a much longer duration. In this study, the corneal surface is irradiated for 10s before the laser is removed. The function $\phi(t)$ may thus be written as

$$\phi(t) = \begin{cases} 1 & \text{for } 0 \leq t \leq 10\text{s}, \\ 0 & \text{for } t > 10\text{s}. \end{cases} \tag{13}$$

The temperature in the cornea at selected points along the pupillary axis at $r = 0$ is plotted against time in Figure 6. During the first two seconds of heating, a rapid increase in corneal temperature is observed. The rate of change of temperature gradually decreases between $t = 2$s and $t = 10$s. At $t > 10$s, following the removal of the laser beam, the heat that is absorbed inside the cornea is diffused rapidly to its surrounding which is illustrated by

the large drop in temperature.

According to Brinkmann *et al* [8], when using continuous wave laser, the cornea must be heated to a minimum temperature of 85°C in order to produce maximum amount of corneal shrinkage. Our model however, only predicted a maximum temperature of approximately 75°C at $(r, z) = (0, 0)$. To produce the maximum amount of shrinkage therefore, one may increase the laser power or prolong the heating duration in order to elevate the corneal temperature to 85°C.

Figure 7 plots the variation of corneal temperature along the pupillary axis (against z at $r = 0$) at $t = 2, 4, 6, 8$ and 10s. Similar to Figure 4, the vertical dotted lines separate the plotted area into the corneal epithelium, corneal stroma and corneal endothelium. The upper (65°C) and lower (55°C) threshold limits for corneal shrinkage to occur is denoted by the horizontal lines.

During the course of laser irradiation, temperature at majority of the stroma is found to lie between 55 and 65°C. At the corneal epithelium, temperature ranges from 65 to 75°C. Comparing this to the temperature produced when using pulsed laser, it appears that the continuous wave laser avoids the problem of over-heating. Similar to pulsed laser heating, no endothelial cell damages are found when the continuous wave laser is used.

Figure 8 plots the spatial temperature profile over a small cross-section of the eye model on the rz plane at $t = 2, 4, 6, 8$ and 10s. As in Figure 5, only cross section where significant changes in temperature can be observed is presented.

6 Discussion and Summary

In the pulsed laser treatment, the temperature profiles in Figures 3 and 4 agree qualitatively with those obtained mathematically by Manns *et al* [12].

The variation of the maximum corneal temperature with time also agrees qualitatively with experimental measurements carried out by Papaioannou *et al* [31]. In the present study, we have not considered the effects of aqueous humor hydrodynamics on the corneal temperature during treatment of L-TKP which were accounted for by Manns *et al* [12]. According to Heys and Barocas [32], there is no significant correlation between the circulation of aqueous humor and heat transfer inside the normal human eye. Since the heating during treatment of L-TKP is localized to a very small region on the cornea, it is not expected to change greatly the circulation inside the aqueous humor. More investigations are necessary to provide further knowledge on the effects of aqueous humor circulation on the corneal surface during treatment of L-TKP.

In the continuous wave laser treatment, the spatial temperature profiles in Figure 8 agree qualitatively with the numerical results demonstrated in [9] and [10]. It should be noted that the intracorneal focusing of the laser modeled by Brinkmann and co-workers [9], [10] is a better model compared to the present one where the laser is assumed to be focused only on the corneal surface. This aspect may be considered in future investigations to further improve the complete eye model presented in this study.

The results in Section 5 do not show corneal relaxation and corneal epithelial damage when L-TKP is carried out using the continuous wave laser. This is however, not the case when the pulsed laser is used. Based on these observations, it appears that the continuous wave laser performs better than the pulsed laser in L-TKP which agrees with the experimental findings in [7] and [33]. In addition to the uniform and homogeneous corneal heating, absence of over-heating and absence of corneal tissue damage, other advantages of the continuous wave laser include minimum heat loss during laser irradiation, requirement of lower energy supply and the tunability of laser wavelength which allows for variation in laser penetration depth [7], [33].

The complete model of the human eye undergoing L-TKP has been successfully developed. This is demonstrated by the good qualitative agreement between the numerical predictions of our model and those obtained from the literature. The use of the boundary element method helps to alleviate the high computational cost required for solving a complete eye model by allowing discretization to be carried out only at the boundaries. In the radially symmetric formulation, the boundary is given by a set of curves which are easily discretized into straight line elements.

In the present work, the boundaries of the eye model are discretized using discontinuous linear elements. Numerical accuracy may be improved by using higher order elements such as the quadratic elements. The formulation of the problem however, may not be as straightforward. Similarly, the accuracy of the time stepping scheme may be improved by using higher order time interpolations instead of the linear one used in this study.

The time-stepping scheme employed in this study appears to perform fairly well. Other methods in dealing with the time dependence of temperature include the use of the time dependent fundamental solution and the Laplace transformation technique. The efficiency and the accuracy of these alternative methods in solving (1) may be explored in future studies.

The main difference between the model in the present study and those found in the literature is in the geometry of the cornea. In earlier studies, the geometry of the cornea which is assumed to be a cylinder or tissue slab with finite thickness is highly idealized. In the present study, the model is anatomically and physiologically more complete and realistic; taking into consideration the various components of the human eye. The use of a complete model provides a more accurate anatomical representation of the human cornea. At the same time, boundary conditions can be specified based on the physical observation of the actual human eye.

The present study is limited to the calculation of temperature changes

during L-TKP which is only the first step for L-TKP. Most of the discussions were carried out based on the temperature that is reached by the cornea during the treatment of L-TKP and thus, may not accurately reflect the actual shrinkage and cell damage phenomena. A more proper analysis will include the calculation of corneal collagen denaturation based on the predicted temperatures from the present model. The stress generated within the cornea due to its shrinkage may also be calculated using the theory of thermoelasticity. These investigations are open for future studies.

Appendix

This section gives the details of the steps involved in the implementation of the boundary element method which include the DR-BEM and the time stepping scheme which are used to obtain a numerical solution of the current problem. The integro-differential equation in (1) is reproduced here as

$$\begin{aligned}\gamma(\xi,\eta)T_i(\xi,\eta,t) = &\int_{\Lambda_i} T_i(r,z,t)\frac{\partial}{\partial n}[\Phi(r,z;\xi,\eta)]\cdot r\cdot ds(r,z)\\ &-\int_{\Lambda_i}\Phi(r,z;\xi,\eta)\frac{\partial}{\partial n}[T_i(r,z,t)]\cdot r\cdot ds(r,z)\\ &+\iint_{R_i}\Phi(r,z;\xi,\eta)\left[\frac{\rho_i c_i}{\kappa_i}\frac{\partial}{\partial t}[T_i(r,z,t)]-\frac{1}{\kappa_i}S_i(r,z,t)\right]dR(r,z)\\ &\text{for } (\xi,\eta)\in R_i\cup\Lambda_i \text{ and } i=1,2,3,4 \text{ and } 5, \qquad \text{(A1)}\end{aligned}$$

For a numerical method based on (A1), we discretize the boundary Λ_i into N_i elements such that $\Lambda_i = \Lambda_i^{(1)}\cup\Lambda_i^{(2)}....\Lambda_i^{(N_i-1)}\cup\Lambda_i^{(N_i)}$. If the starting and ending points (r,z) of the element $\Lambda_i^{(k)}$ (for $k=1,2,...,N_i-1,N_i$) are denoted by $(r_i^{(k)},z_i^{(k)})$ and $(r_i^{(k+1)},z_i^{(k+1)})$ respectively, we choose two points

on $\Lambda_i^{(k)}$ such that

$$(\xi_i^{(k)}, \eta_i^{(k)}) = (r_i^{(k)}, z_i^{(k)}) + \tau \left(r_i^{(k+1)} - r_i^{(k)}, z_i^{(k+1)} - z_i^{(k)} \right)$$
$$(\xi_i^{(k+N_i)}, \eta_i^{(k+N_i)}) = (r_i^{(k)}, z_i^{(k)}) + (1-\tau)(r_i^{(k+1)} - r_i^{(k)}, z_i^{(k+1)} - z_i^{(k)}), \qquad \text{(A2)}$$

where τ may be any pre-selected real number such that $0 < \tau < 0.5$. For the purpose of obtaining the results presented in Section 5, τ is taken to be 0.25.

The temperature and heat flux ($-\kappa \partial T/\partial n = q$) on $\Lambda_i^{(k)}$ are approximated by

$$T_i(r,z,t) \simeq \frac{\left[s_i^{(k)}(r,z) - (1-\tau)\,\ell_i^{(k)} \right] T_i^{(k)}(t) - \left[s_i^{(k)}(r,z) - \tau \ell_i^{(k)} \right] T_i^{(k+N_i)}(t)}{(2\tau - 1)\,\ell_i^{(k)}} \quad \text{for } (r,z) \in \Lambda_i^{(k)}, \qquad \text{(A3)}$$

and

$$q_i(r,z,t) \simeq \frac{\left[s_i^{(k)}(r,z) - (1-\tau)\,\ell_i^{(k)} \right] q_i^{(k)}(t) - \left[s_i^{(k)}(r,z) - \tau \ell_i^{(k)} \right] q_i^{(k+N_i)}(t)}{(2\tau - 1)\,\ell_i^{(k)}} \quad \text{for } (r,z) \in \Lambda_i^{(k)}, \qquad \text{(A4)}$$

where $T_i^{(k)}(t)$ and $T_i^{(k+N)}(t)$ are the temperature at the points $(\xi_i^{(k)}, \eta_i^{(k)})$ and $(\xi_i^{(k+N_i)}, \eta_i^{(k+N_i)})$ respectively, $q_i^{(k)}(t)$ and $q_i^{(k+N)}(t)$ are the heat flux at $(\xi_i^{(k)}, \eta_i^{(k)})$ and $(\xi_i^{(k+N_i)}, \eta_i^{(k+N_i)})$ respectively, $\ell_i^{(k)}$ is the length of element $\Lambda_i^{(k)}$ and $s_i^{(k)}(r,z)$ is defined as

$$s_i^{(k)}(r,z) = \sqrt{\left(r - r_i^{(k)} \right)^2 + \left(z - z_i^{(k)} \right)^2} \text{ for } (r,z) \in \Lambda_i^{(k)}. \qquad \text{(A5)}$$

In (A3) and (A4), note that T_i and q_i are approximated as linear functions of $s_i^{(k)}$ across the element $\Lambda_i^{(k)}$.

Substituting (A3) and (A4) into (A1) gives

$$\begin{aligned}\gamma(\xi,\eta)T_i(\xi,\eta,t) = &\sum_{k=1}^{N_i}\frac{1}{(2\tau-1)\,\ell_i^{(k)}}\\ &\times\Big\{\Big[-(1-\tau)\,\ell_i^{(k)}G_{2i}^{(k)}(\xi,\eta)+G_{4i}^{(k)}(\xi,\eta)\Big]\,T_i^{(k)}(t)\\ &+\Big[\tau\ell_i^{(k)}G_{2i}^{(k)}(\xi,\eta)-G_{4i}^{(k)}(\xi,\eta)\Big]\,T_i^{(k+N_i)}(t)\\ &-\Big[-(1-\tau)\,\ell_i^{(k)}G_{1i}^{(k)}(\xi,\eta)+G_{3i}^{(k)}(\xi,\eta)\Big]\,q_i^{(k)}(t)\\ &-\Big[\tau\ell_i^{(k)}G_{1i}^{(k)}(\xi,\eta)-G_{3i}^{(k)}(\xi,\eta)\Big]\,q_i^{(k+N_i)}(t)\Big\}\\ &+\iint_{R_i}\Phi(r,z;\xi,\eta)\left[\frac{\rho_i c_i}{\kappa_i}\frac{\partial}{\partial t}[T_i(r,z,t)]-\frac{1}{\kappa_i}S_i(r,z,t)\right]dR(r,z)\end{aligned}$$

$$\text{for } (\xi,\eta)\in R_i\cup\Lambda_i \text{ and } i=1,2,3,4 \text{ and } 5, \quad \text{(A6)}$$

where

$$\begin{aligned}G_{1i}^{(k)}(\xi,\eta) &= \int_{\Lambda_i^{(k)}}\Phi(r,z;\xi,\eta)\cdot r\cdot ds(r,z),\\ G_{2i}^{(k)}(\xi,\eta) &= \int_{\Lambda_i^{(k)}}\frac{\partial}{\partial n}[\Phi(r,z;\xi,\eta)]\cdot r\cdot ds(r,z),\\ G_{3i}^{(k)}(\xi,\eta) &= \int_{\Lambda_i^{(k)}}s_i^{(k)}(r,z)\,\Phi(r,z;\xi,\eta)\cdot r\cdot ds(r,z),\\ G_{4i}^{(k)}(\xi,\eta) &= \int_{\Lambda_i^{(k)}}s_i^{(k)}(r,z)\,\frac{\partial}{\partial n}[\Phi(r,z;\xi,\eta)]\cdot r\cdot ds(r,z). \qquad \text{(A7)}\end{aligned}$$

The integrals in (A7) may be calculated numerically by using, for example, Gaussian quadrature.

The domain integral in (A6) may be converted into a boundary integral using the DR-BEM [34]. To do so, L_i points denoted by $(\xi_i^{(2N_i+1)},\eta_i^{(2N_i+1)})$, $(\xi_i^{(2N_i+2)},\eta_i^{(2N_i+2)})$, ..., $(\xi_i^{(2N_i+L_i-1)},\eta_i^{(2N_i+L_i-1)})$ and $(\xi_i^{(2N_i+L_i)},\eta_i^{(2N_i+L_i)})$ (for

$i = 1, 2, 3, 4$ and 5), are selected in the interior of R_i. These points serve as collocation points for the DR-BEM. Besides the interior collocation points, the $2N_i$ boundary points on the boundary elements of Λ_i, as defined in (A2), are also used.

In the DR-BEM, the domain integral is approximated by

$$\iint_{R_i} \Phi(r,z;\xi,\eta)\left[\frac{\rho_i c_i}{\kappa_i}\frac{\partial}{\partial t}[T_i(r,z,t)] - \frac{1}{\kappa_i}S_i(r,z,t)\right] dR(r,z)$$
$$\simeq \sum_{m=1}^{2N_i+L_i}\left[\frac{\rho_i c_i}{\kappa_i}\frac{d}{dt}[T_i^{(m)}(t)] - \frac{1}{\kappa_i}S_i(r,z,t)\right]\sum_{j=1}^{2N_i+L_i} W_i^{(mj)}\Psi_i^{(j)}(\xi,\eta)$$
$$\text{for } i = 1, 2, 3, 4 \text{ and } 5 \qquad \text{(A8)}$$

where $T_i^{(m)}(t) = T_i(\xi_i^{(m)}, \eta_i^{(m)}, t)$ for $m = 1,\ 2,\ \cdots,\ 2N_i + L_i$ and the coefficients $W_i^{(mj)}$ and $\Psi_i^{(j)}(\xi,\eta)$ are defined implicitly by

$$\sum_{j=1}^{2N_i+L_i} W_i^{(kj)}\theta_i^{(p)}(\xi_i^{(j)}, \eta_i^{(j)}) = \begin{cases} 0 & \text{if} \quad p \neq k \\ 1 & \text{if} \quad p = k \end{cases} \quad \text{for } p,\ k = 1, 2, \cdots, 2N_i + L_i, \qquad \text{(A9)}$$

and

$$\Psi_i^{(j)}(\xi,\eta) = \gamma(\xi,\eta)\chi_i^{(j)}(\xi,\eta) - \int_{\Lambda_i} \chi_i^{(j)}(\xi,\eta)\frac{\partial}{\partial n}[\Phi(r,z;\xi,\eta)]\cdot r\cdot ds(r,z)$$
$$+ \int_{\Lambda_i} \Phi(r,z;\xi,\eta)\frac{\partial}{\partial n}[\chi_i^{(j)}(\xi,\eta)]\cdot r\cdot ds(r,z)$$
$$\text{for } j = 1, 2....2N_i + L_i, \qquad \text{(A10)}$$

respectively. The local interpolating function, $\theta_i^{(p)}$ and the particular solution, $\chi_i^{(j)}$ may be expressed as

$$\theta_i^{(p)}(r,z) = 4E(m(r,z;\xi_i^{(p)},\eta_i^{(p)}))\sqrt{a(r,z;\xi_i^{(p)},\eta_i^{(p)}) + b(r;\xi_i^{(p)})} \qquad \text{(A11)}$$

and

$$\chi_i^{(p)}(\xi,\eta) = \frac{1}{9}(a(r,z;\xi_i^{(p)},\eta_i^{(p)}) + b(r;\xi_i^{(p)}))\sqrt{a(r,z;\xi_i^{(p)},\eta_i^{(p)}) + b(r;\xi_i^{(p)})}$$
$$\times [(m(r,z;\xi_i^{(p)},\eta_i^{(p)}) - 1)K(m(r,z;\xi_i^{(p)},\eta_i^{(p)}))$$
$$+ (4 - 2m(r,z;\xi_i^{(p)},\eta_i^{(p)}))E(m(r,z;\xi_i^{(p)},\eta_i^{(p)}))] \tag{A12}$$

respectively. Details on the functions in (A11) and (A12) may be found in [35].

Substituting (A8) into (A6) and letting (ξ,η) be given by $(\xi_i^{(n)},\eta_i^{(n)})$, one obtains

$$\begin{aligned}
&\gamma(\xi_i^{(n)},\eta_i^{(n)})T_i^{(n)}(t) \\
&= \sum_{k=1}^{N_i} \frac{1}{(2\tau-1)\,\ell_i^{(k)}} \\
&\times \left\{ \left[-(1-\tau)\,\ell_i^{(k)} G_{2i}^{(k)}(\xi_i^{(n)},\eta_i^{(n)}) + G_{4i}^{(k)}(\xi_i^{(n)},\eta_i^{(n)}) \right] T_i^{(k)}(t) \right. \\
&+ \left[\tau \ell_i^{(k)} G_{2i}^{(k)}(\xi_i^{(n)},\eta_i^{(n)}) - G_{4i}^{(k)}(\xi_i^{(n)},\eta_i^{(n)}) \right] T_i^{(k+N_i)}(t) \\
&- \left[-(1-\tau)\,\ell_i^{(k)} G_{1i}^{(k)}(\xi_i^{(n)},\eta_i^{(n)}) + G_{3i}^{(k)}(\xi_i^{(n)},\eta_i^{(n)}) \right] q_i^{(k)}(t) \\
&- \left. \left[\tau \ell_i^{(k)} G_{1i}^{(k)}(\xi_i^{(n)},\eta_i^{(n)}) - G_{3i}^{(k)}(\xi_i^{(n)},\eta_i^{(n)}) \right] q_i^{(k+N_i)}(t) \right\} \\
&+ \sum_{m=1}^{2N_i+L_i} \left[\frac{\rho_i c_i}{\kappa_i} \frac{d}{dt}[T_i^{(m)}(t)] - \frac{1}{\kappa_i} S_i(r,z,t) \right] \\
&\times \sum_{j=1}^{2N_i+L_i} W_i^{(mj)} \Psi_i^{(j)}(\xi_i^{(n)},\eta_i^{(n)}) \\
&\qquad \text{for } n = 1, 2 \ldots 2N_i + L_i - 1, 2N_i + L_i \\
&\qquad\qquad \text{and } i = 1, 2, 3, 4 \text{ and } 5.
\end{aligned} \tag{A13}$$

The function $T_i^{(m)}(t)$ and its first order derivative are approximated using

$$T_i^{(m)}(t) \simeq \frac{1}{2}\left[T_i^{(m)}(t+\frac{1}{2}\Delta t) + T_i^{(m)}(t-\frac{1}{2}\Delta t)\right],$$
$$\frac{d}{dt}[T_i^{(m)}(t)] \simeq \frac{1}{\Delta t}\left[T_i^{(m)}(t+\frac{1}{2}\Delta t) - T_i^{(m)}(t-\frac{1}{2}\Delta t)\right], \qquad \text{(A14)}$$

where Δt is a small positive number. Note the magnitudes of the errors in the approximations above are $O([\Delta t]^2)$.

Substituting the approximation in (A14) into (A13) gives

$$\begin{aligned}
&\frac{1}{2}\gamma(\xi_i^{(n)},\eta_i^{(n)})[T_i^{(n)}(t+\frac{1}{2}\Delta t) + T_i^{(n)}(t-\frac{1}{2}\Delta t)] \\
&= \sum_{k=1}^{N_i} \frac{1}{(2\tau-1)\,\ell_i^{(k)}} \\
&\times \left\{ \frac{1}{2}\left[-(1-\tau)\,\ell_i^{(k)} G_{2i}^{(k)}(\xi_i^{(n)},\eta_i^{(n)}) + G_{4i}^{(k)}(\xi_i^{(n)},\eta_i^{(n)})\right]\right. \\
&\times \left[T_i^{(k)}(t+\frac{1}{2}\Delta t) + T_i^{(k)}(t-\frac{1}{2}\Delta t)\right] \\
&+ \frac{1}{2}\left[\tau\ell_i^{(k)} G_{2i}^{(k)}(\xi_i^{(n)},\eta_i^{(n)}) - G_{4i}^{(k)}(\xi_i^{(n)},\eta_i^{(n)})\right] \\
&\times \left[T_i^{(k+N_i)}(t+\frac{1}{2}\Delta t) + T_i^{(k+N_i)}(t-\frac{1}{2}\Delta t)\right] \\
&- \left[(1-\tau)\,\ell_i^{(k)} G_{1i}^{(k)}(\xi_i^{(n)},\eta_i^{(n)}) + G_{3i}^{(k)}(\xi_i^{(n)},\eta_i^{(n)})\right] q_i^{(k)}(t) \\
&\left.- \left[\tau\ell_i^{(k)} G_{1i}^{(k)}(\xi_i^{(n)},\eta_i^{(n)}) - G_{3i}^{(k)}(\xi_i^{(n)},\eta_i^{(n)})\right] q_i^{(k+N_i)}(t)\right\} \\
&+ \sum_{m=1}^{2N_i+L_i}\left[\frac{\rho_i c_i}{\kappa_i \Delta t}\left(T_i^{(m)}(t+\frac{1}{2}\Delta t) - T_i^{(m)}(t-\frac{1}{2}\Delta t)\right) - \frac{1}{\kappa_i}S_i(r,z,t)\right] \\
&\times \sum_{j=1}^{2N_i+L_i} W_i^{(mj)}\Psi_i^{(j)}(\xi_i^{(n)},\eta_i^{(n)})
\end{aligned}$$

$$\text{for } n = 1, 2 \ldots 2N_i + L_i - 1, 2N_i + L_i$$
$$\text{and } i = 1, 2, 3, 4 \text{ and } 5. \qquad \text{(A15)}$$

If $T_i^{(m)}(t-\frac{1}{2}\Delta t)$ is assumed known, then (A15) together with (5), (6) and (7) can be reduced to a system of $2 \times (N_1 + N_2 + N_3 + N_4 + N_5) + (L_1 +$

$L_2 + L_3 + L_4 + L_5$) algebraic equations in $2 \times (N_1 + N_2 + N_3 + N_4 + N_5) + (L_1 + L_2 + L_3 + L_4 + L_5)$ unknown functions of t. The non-linear boundary condition in (5) is treated using the iterative procedure outlined in [17] so that the system of algebraic equations to solve is a linear one. With $T_i^{(m)}(0)$ given by the steady-state temperature prior to the laser heating, the linear system is solved by letting $t = \frac{1}{2}\Delta t, \frac{3}{2}\Delta t, \frac{5}{2}\Delta t$, ..., in a consecutive manner, to determine the unknown functions of t at higher and higher time levels.

References

[1] Laser thermokeratoplasty the ideal choice for presbyopes?, *Ophthalmology Times Europe*, 2008: http://www.oteurope.com /ophthalmologytimeseurope /Refractive /Laser-thermokeratoplasty-the-ideal-choice-for-pres/ArticleStandard/Article/ detail/489477 (last accessed: 31st March 2008)

[2] N.A Peppers, A. Vassiliadis, K.G Dedrick, H. Chang, R.R Peabody, H. Rose and H.C Zweng, Corneal damage threshold for CO_2 Laser Irradiation. *Applied Optics*, **8 (2)**, pp. 377-381, 1969

[3] M.A Mainster, Ophthalmic applications of infrared lasers-thermal considerations. *Investigative Ophthalmology for Visual Science*, **18 (4)**, pp. 414-420, 1979.

[4] M.A Mainster, T.J White and J.H Tips, Corneal thermal response to the CO_2 Laser. *Applied Optics*, **9 (3)**, pp. 665-667, 1970.

[5] Z. Zhou, Q. Ren, G. Simon and J.M Parel, Thermal modeling of Laser Photo Thermal Keratoplasty (LPTK). In: J.M Parel, eds, *Ophthalmic Technologies II, Proceedings of the SPIE*, **1644**, pp.61-71, 1992.

[6] R. Brinkmann, N. Koop, G. Dröge, U. Grotehusmann, A. Huber and R. Birngruber, Investigations on Laser Thermokeratoplasty. In: S.T Melamed, eds, *Laser Applications in Ophthalmology, Proceedings of the SPIE,* **2079**, pp. 120-130, 1994.

[7] R. Brinkmann, J. Kampmeier, U. Grotehusmann, A. Vogel, N. Koop, M.A Vogel and R. Birngruber, Corneal collagen denaturation in Laserthermokeratoplasty, In: S.L Jacques, *Laser-Tissue Interaction VII, Proceedings of the SPIE*, **2681**, pp. 56-62, 1996.

[8] R. Brinkmann, N. Koop, K. Kamm, G. Geerling, J. Kampmeier and R. Birngruber, Laser thermokeratoplasty by maens of a continuously emitting laser diode in the mid-IR. In: R. Birngruber, A.F Fercher, P. Sourdille, *Lasers in Ophthalmology IV, Proceedings of the SPIE*, **2930**, pp. 66-74, 1996.

[9] R. Brinkmann, G. Geerling, J. Kampmeier, N. Koop, B. Radt and R. Birngruber, Laser thermokeratoplasty: Analysis of in vitro results and refractive changes achieved in a first clinical study. In: G. Altshuler, R. Birngruber, M.D Fante, R. Hibst, H. Hoenigsmann, N. Krasner and F. Laffitte, *Medical Applications of Lasers in Dermatology, Ophthalmology, Dentistry, and Endoscopy, Proceedings of the SPIE*, **3192**, pp. 180-186, 1997.

[10] R. Brinkmann, B. Radt, C. Flamm, J. Kampmeier, N. Koop and R. Birngruber, Influence of temperature and time on thermally induced forces in corneal collagen and the effect on laser thermokeratoplasty. *Journal of Cataract and Refractive Surgery*, **26 (5)**, pp. 744-754, 2000.

[11] F. Manns, D. Borja and J.M Parel, Calculation of corneal temperature and shrinkage during Laser Thermokeratoplasty (LTK). In: F. Manns,

P.G Söderberg and A. Ho, eds, *Ophthalmic Technologies XII, Proceedings of the SPIE*, **4611**, pp. 101-109, 2002.

[12] F. Manns, D. Borja and J.M Parel, Semianalytical thermal model for subablative laser heating of homogeneous nonperfused biological tissue: application to laser thermokeratoplasty. *Journal of Biomedical Optics*, **8 (2)**, pp. 288-297, 2003.

[13] A.S Podol'stev and G.I Zheltov, Photodestructive effect of IR laser radiation on the cornea, *Geometrical and Applied Optics*, 102 (1), pp. 142-146, 2007.

[14] H. Stringer and J. Parr, Shrinkage temperature of eye collagen, *Nature*, **204 (4695)**, pp. 1307, 1964.

[15] E. Spoerl, K. Schmalfuss, U. Genth, T. Seiler and H.J Huebscher, Thermo-mechanical behaviour of the cornea. *Investigative Ophthalmology and Visual Science*, **36 (4)**, pp. 39, 1995.

[16] C. Wirbelauer, G. Geerling, N. Koop, R. Brinkmann, A. Tüngler, R. Birngruber and H. Laqua, Acute endothelial cell changes after laser thermal keratoplasty with a cw-IR laser diode. *Investigative Ophthalmology and Visual Science*, **38 (4)**, pp. 541, 1997.

[17] E.H Ooi, W.T Ang and E.Y.K Ng, Bioheat transfer in the human eye: A boundary element approach" *Engineering Analysis with Boundary Elements*, **31 (6)**, pp. 494-500, 2007.

[18] M.W Charles and N. Brown, Dimensions of the human eye relevant to radiation protection. *Physics in Medicine and Biology*, **20 (2)**, pp. 202-218, 1975.

[19] S.T Fontana and R.F Brubaker, Volume and dof the anterior chamber of the normal aging human eye. *Archives of Ophthalmology*, **98 (10)**, pp. 1803-1808, 1980.

[20] U. Cicekli, Computational model for heat transfer in the human eye using the finite element method (M.Sc thesis, Department of Civil & Environmental Engineering, Louisiana State University), 2003.

[21] A.F Emery, P.O Kramar, A.W Guy and J.C Lin, Microwave induced temperature rises in rabbit eyes in cataract research. *Journal of Heat Transfer*, **97**, pp. 123-128, 1975.

[22] J.A Scott, A finite element model of heat transport in the human eye. *Physics in Medicine and Biology*, **33 (2)**, pp. 227-24, 1988.

[23] P.S Neelakantaswamy and K.P Ramakrishnan, Microwave-induced hazardous nonlinear thermoelastic vibrations of the ocular lens in the human eye. *Journal of Biomechanics*, **12 (3)**, pp. 205-210, 1979.

[24] J.J.W Lagendijk, A mathematical model to calculate temperature distributions in human and rabbit eyes during hyperthermic treatment. *Physics in Medicine and Biology*, **27 (11)**, pp. 1301-1311, 1982.

[25] D. Sliney and M. Wolbarsht, *Safety With Lasers and Other Optical Sources: A Comprehensive Handbook, Plenum Press*, New York, 1980.

[26] E.Y.K Ng and E.H Ooi, FEM simulation of the eye structure with bioheat analysis. *Computer Methods and Programs in Biomedicine*, **82 (3)**, pp. 268-276, 2006.

[27] M. Abramowitz and I. Stegun, *Handbook of Mathematical Functions*, Dover, New York, 1972.

[28] C.A Brebbia, J.C.F Telles and L.C Wrobel, *Boundary Element Techniques: Theory and Applications in Engineering*. Berlin/Heidelberg: Springer, 1984.

[29] MATLAB 6.5: http://www.mathworks.com/products/matlab (last accessed: 31st March 2008)

[30] P.L Kaufman and A. Alm, *Adler's Physiology of the Eye: Clinical Application*, 10th Edition, St. Louis, MO: Mosby, 2003.

[31] T. Papaioannou, E. Maguen and W.S. Grundfest, Spatiotemporal temperature profiling of corneal surface during LTK, In: F. Manns, P.G Söderberg and A. Ho, eds, *Ophthalmic Technologies XII, Proceedings of the SPIE*, **4611**, pp. 110-114, 2002.

[32] J.J Heys and V.H Barocas, A Boussinesq model of natural convection in the human eye and the formation of Krukenberg's Spindle. *Annals of Biomedical Engineering*, **30 (3)**, pp. 392-401, 2002.

[33] B. Jean, T. Bende, T. Oltrup, M. Matallana and R. Walker, Depth adjusted thermal keratoplasty using a cw diode laser and a new focusing handpiece. In: J.M Parel, K.M Joos, P.O Rol, *Ophthalmic Technologies VI, Proceedings of the SPIE*, **2673**, pp. 61-67, 1996.

[34] C.A Brebbia and D. Nardini D, Dynamic analysis in solid mechanics by an alternative boundary element procedure. *Engineering Analysis with Boundary Elements*, **24 (7)**, pp. 228-233, 2000.

[35] K. Wang, R. M. M. Mattheij and H. G. ter Morsche, Alternative DRM formulations. *Engineering Analysis with Boundary Elements*, **27 (2)**, pp. 175-181, 2003.

List of tables and figures

Table 1: Thermal properties of each eye region

Region	**Thermal conductivity,** κ ($\mathrm{Wm^{-1}K^{-1}}$)	**Density,** ρ ($\mathrm{kgm^{-3}}$)	**Specific heat,** c ($\mathrm{Jkg^{-1}K^{-1}}$)
Cornea, R_1	0.58 [21]	1050 [22]	4178 [23]
Aqueous humor, R_2	0.58 [21]	996 [22]	3997 [22]
Lens, R_3	0.40 [24]	1050 [23]	3000 [24]
Vitreous, R_4	0.60 [22]	1000 [22]	4178 [22]
Sclera, R_5	1.00 [20]	1100 [20]	3180 [20]

Table 2: Parameters in the boundary conditions

Parameter	**Value**
Blood temperature, T_{bl} (^{o}C)	37
Ambient temperature T_{amb} (^{o}C)	25
Blood convection coefficient, h_{bl} ($\mathrm{Wm^{-2}K^{-1}}$)	65
Ambient convection coefficient, h_{amb} ($\mathrm{Wm^{-2}K^{-1}}$)	10
Evaporation rate, E_{vap} ($\mathrm{Wm^{-2}}$)	40
Emissivity of the cornea, ε	0.975
Stefan-Boltzmann constant, σ ($\mathrm{Wm^{-2}K^{-4}}$)	5.67×10^{-8}

Table 3: Typical laser parameters chosen for the pulsed laser

Parameter	**Value**
Energy per pulse (mJ)	30
Pulse duration (μs)	200
Peak irradiance, E_0 (Wm^{-2})	5.31×10^8
Pulse repetition rate (Hz)	5
Wavelength (μm)	2.1
Laser absorption coefficient of water, μ (m^{-1})	2000

Table 4: Typical laser parameters chosen for the continuous wave laser

Parameter	**Value**
Laser power, P (mW)	125
Peak irradiance, E_0 (Wm^{-2})	4.42×10^5
Heating duration (s)	10
Wavelength (μm)	1.87
Laser absorption coefficient of water, μ (m^{-1})	1900

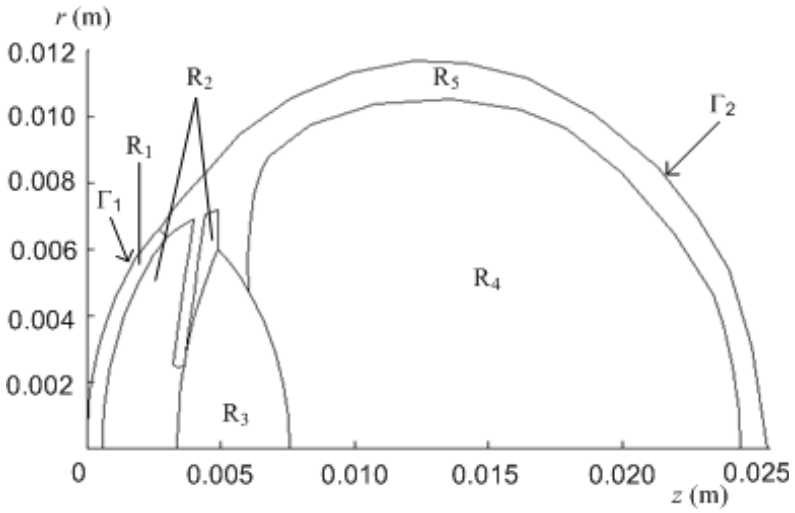

Figure 1: The human eye model

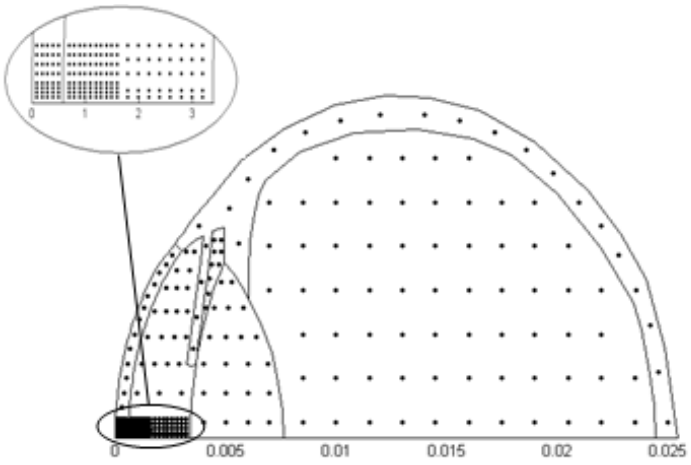

Figure 2: Interior collocation points selected for the eye model

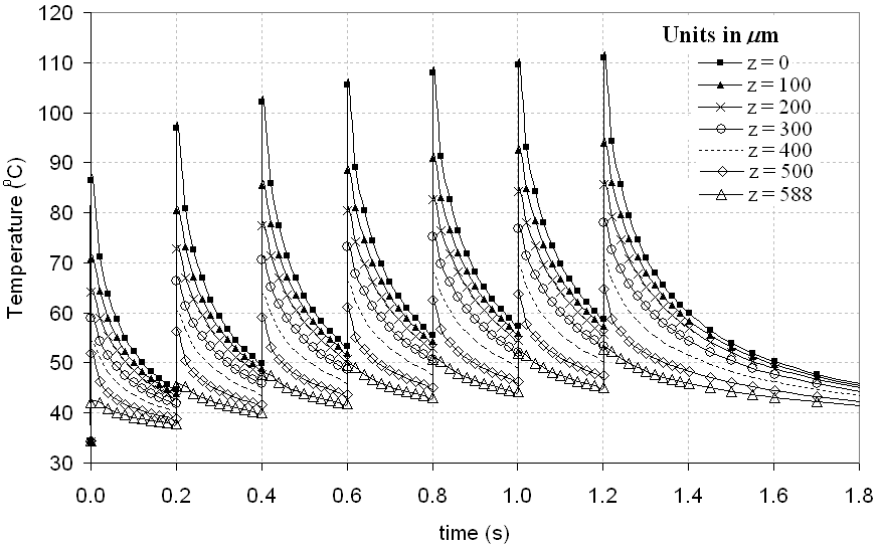

Figure 3: Plots of the corneal temperature against time at various points along the pupiliary axis ($r = 0$) during pulsed laser irradiation

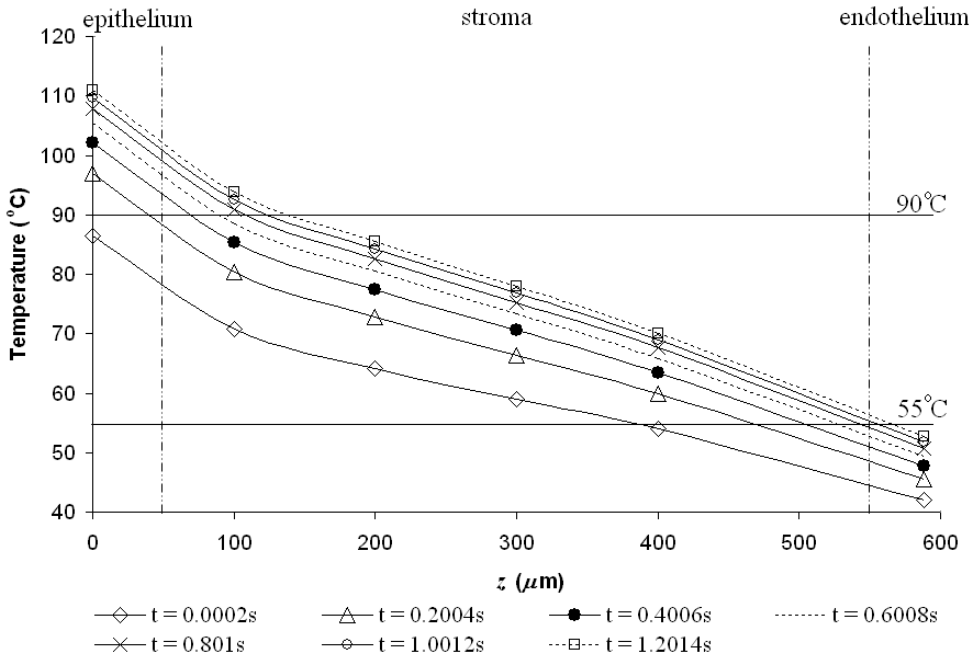

Figure 4: The corneal temperature along the pupiliary axis (against z at $r = 0$) at the end of each laser pulse

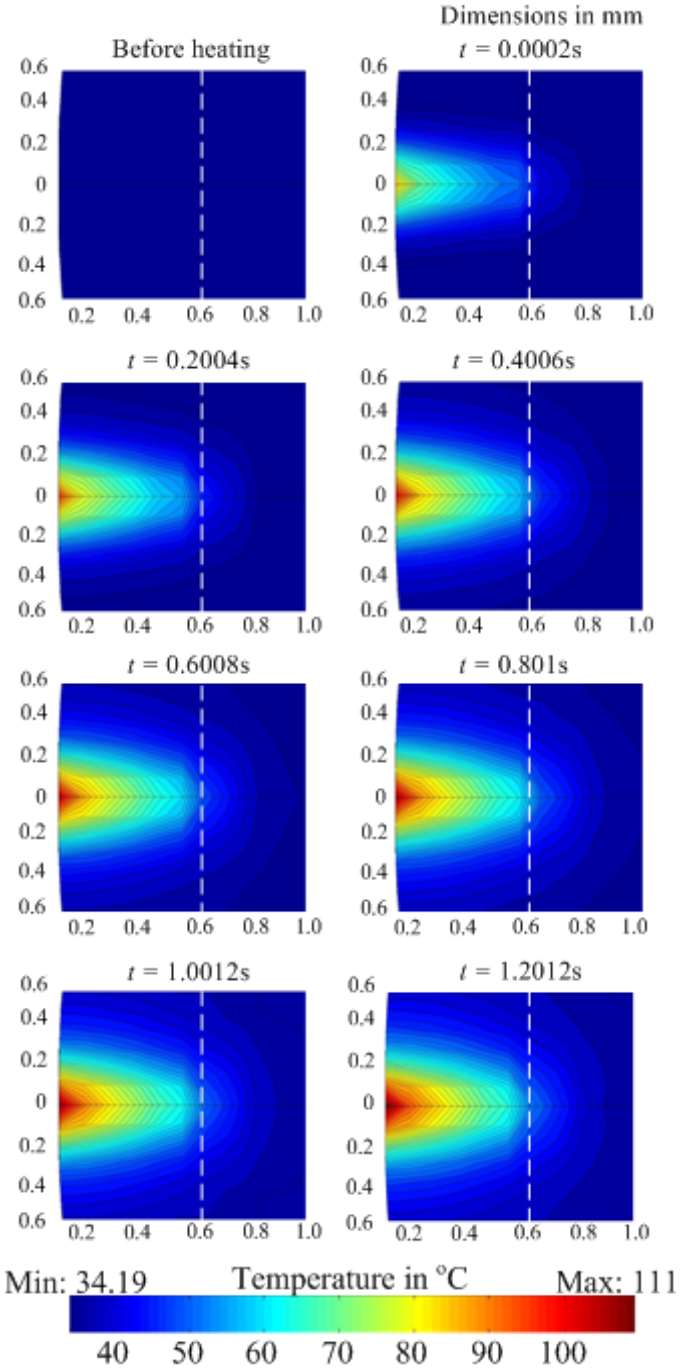

Figure 5: Spatial temperature profiles over a selected cross-section of the eye subject to pulsed laser irradiation

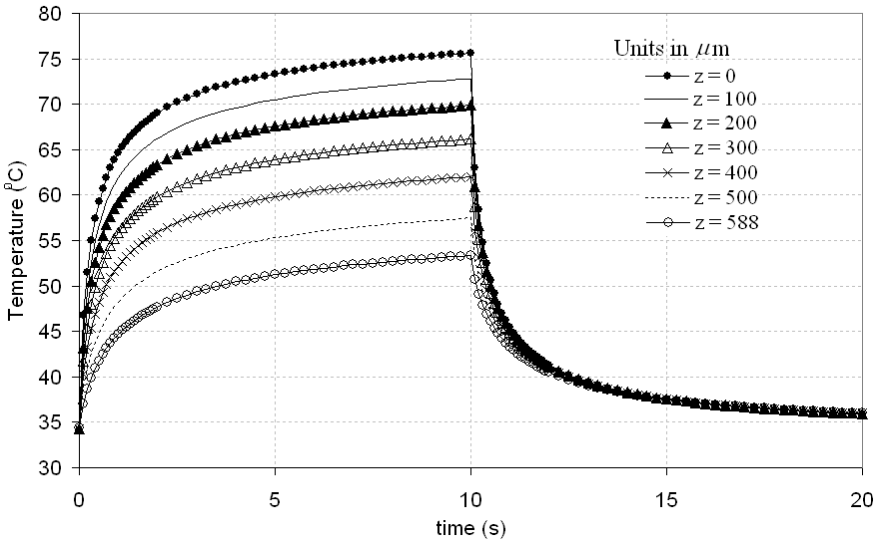

Figure 6: Temperature against time at selected points along the pupiliary axis

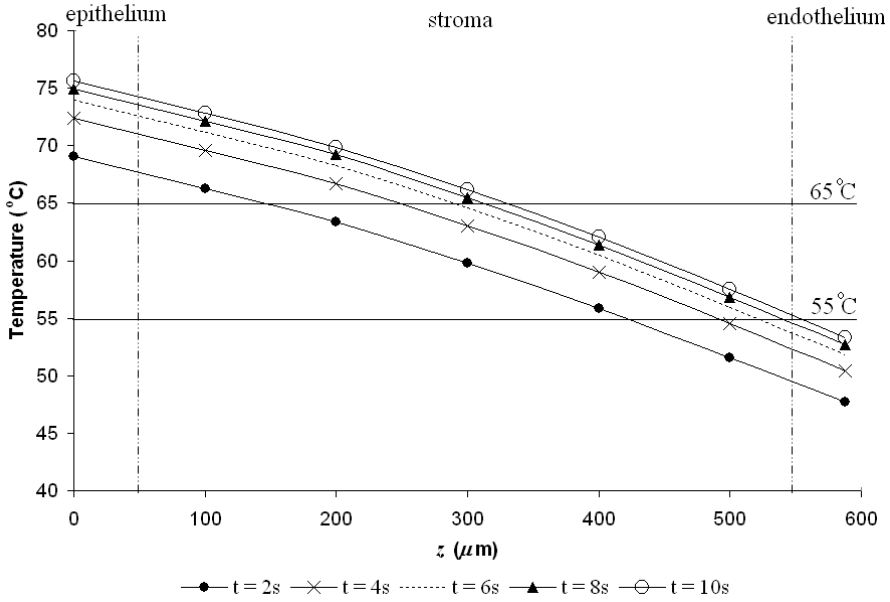

Figure 7: The corneal temperature along the pupiliary axis (against z at $r = 0$) at various time levels

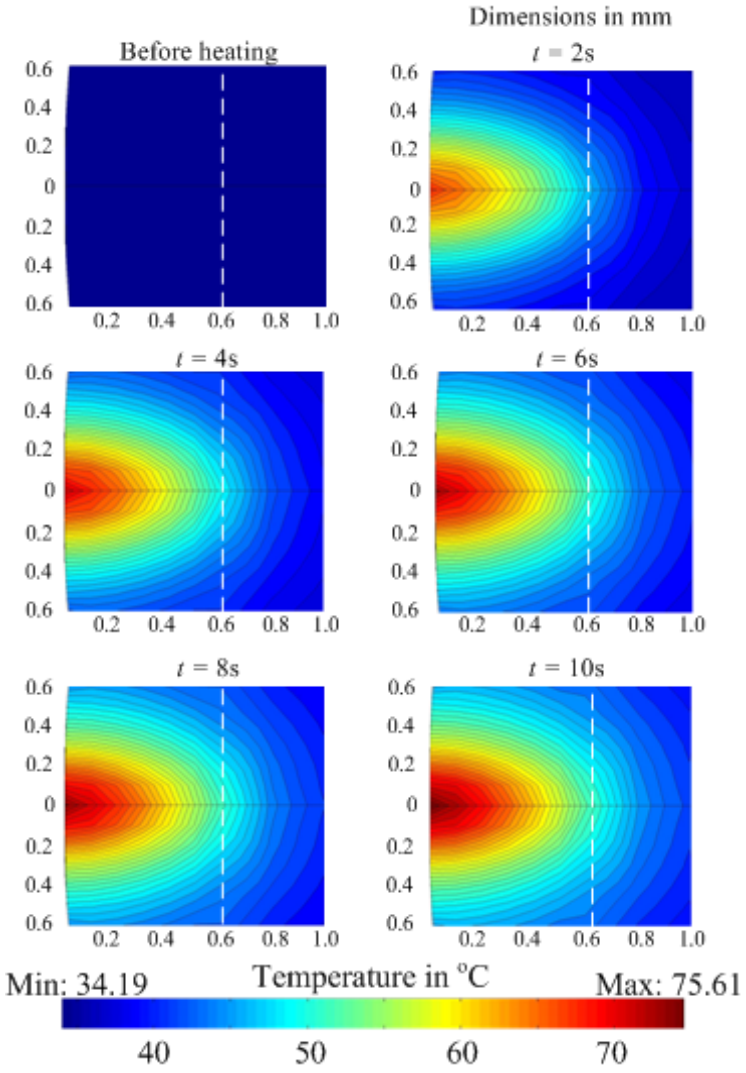

Figure 8: Spatial temperature profile over a small cross-section of the eye during continuous wave laser irradiation